

# InSAR analysis of the 2008 Reno-Mogul earthquake swarm: Evidence for westward migration of Walker Lane style dextral faulting

John W. Bell,<sup>1</sup> Falk Amelung,<sup>2</sup> and Christopher D. Henry<sup>1</sup>

Received 21 June 2012; revised 14 August 2012; accepted 15 August 2012; published 26 September 2012.

[1] Analysis and modeling of InSAR data covering the 2008 Reno-Mogul M 4.7 earthquake swarm indicate that the main event was produced by slip on a previously unrecognized strike-slip fault in the Reno basin. Deformation of 0.5–2.5 cm in radar line-of-sight was produced by the main event and post-seismic slip over an area of more than  $\sim 150$  km<sup>2</sup>. This earthquake is one of the smallest magnitude events modeled with InSAR to date in the seismically active western Basin and Range, and it provides new insights into regional neotectonic relations. Inverse modeling of the InSAR data suggests that the earthquake swarm was generated by 25–75 cm of dextral displacement on a N44W-striking fault with a  $\sim 3$  km rupture length and a rupture depth of  $\sim 2$  km. The InSAR-detected strike-slip ground deformation is unique for the Reno basin which is in the purely extensional domain of the Sierra Nevada-Basin and Range Transition Zone, an area dominated by north-striking normal faults. The InSAR modeling of the 2008 earthquake swarm supports the concept of westward migration of Walker Lane transcurrent faulting and overprinting of extensional Basin and Range structures, in this case the westward migration of dextral shear associated with the northern Walker Lane into the extension-dominated Reno basin. **Citation:** Bell, J. W., F. Amelung, and C. D. Henry (2012), InSAR analysis of the 2008 Reno-Mogul earthquake swarm: Evidence for westward migration of Walker Lane style dextral faulting, *Geophys. Res. Lett.*, 39, L18306, doi:10.1029/2012GL052795.

## 1. Introduction

[2] In February, 2008, a swarm of small magnitude (M 1–4), shallow (<2–3 km) earthquakes began near Mogul, Nevada, 10 km west of Reno [Smith *et al.*, 2008] (Figures 1a and 1b). The swarm activity increased in intensity, including several M 3–4 events, and culminated in an M 4.7 ( $M_w$  5.0) main event on April 25, 2008. Following the main shock, post-seismic swarm activity continued at a similar rate through August, 2008 by which time thousands of  $M > 1$  events had occurred. Well-constrained waveform mechanisms indicated that the main event was caused by dextral slip on a concealed northwest-striking fault at the northern end of the Carson

Range, the northernmost block of the Sierra Nevada [Smith *et al.*, 2008] (Figure 1b and Figure S1 in the auxiliary material).<sup>1</sup> The Mogul swarm was similar to earlier regional swarms [dePolo *et al.*, 2008], but the M 4.7 earthquake was unusual because it was a strike-slip event that occurred within a purely extensional domain of the western Basin and Range. Published geologic mapping had not identified any major northwest-striking, late Cenozoic structures [Bell and Garside, 1987; Henry and Perkins, 2001] or any Quaternary faults (U.S. Geological Survey, Quaternary fault and fold database for the United States, 2006, accessed 20 January 2010, available at <http://earthquake.usgs.gov/regional/faults>) that could account for the strike-slip event.

[3] InSAR analyses have been most commonly used to detect and model fault motion associated with large magnitude earthquakes [cf. Massonnet *et al.*, 1993]. In this study, we use InSAR to detect the ground deformation associated with the M 4.7 main event and post-seismic slip. Our results show that InSAR can be successfully used to model such small tectonic events thereby providing new insights into tectonic processes and evolutionary trends within the Basin and Range.

## 2. Structural-Tectonic Setting

[4] The western Basin and Range underwent post-mid-Miocene east-west extension followed by transcurrent faulting associated with the development of the Walker Lane, a 700-km-long zone of predominantly northwest-striking dextral faults [Stewart, 1988]. The Walker Lane accommodates northwest translation of the Sierra Nevada and 20–25% of Pacific-North American plate motion [Hammond and Thatcher, 2007]. It has been propagating northward from southern Nevada and southeastern California as an incipient plate-boundary-like structure since about 13 Ma, overprinting extensional Basin and Range structures [Faulds *et al.*, 2005].

[5] The Reno basin is dominated by this post-mid-Miocene extension, near the boundary with the relatively stable Sierra Nevada and west of the northern Walker Lane (Figures 1a and S2) [Stewart, 1988; Faulds and Henry, 2008]. The Sierra Nevada-Basin and Range transition zone underwent two episodes of east-west extension at  $\sim 12$  and 3 Ma [Henry and Perkins, 2001; Stockli *et al.*, 2003]. The 3 Ma episode generated a series of north-striking half graben bounded by major normal faults. The Reno basin is one such half graben, bounded on the east by west-dipping normal faults (Figure 1b). The Carson Range is a north-plunging, extensional anticline bounded on the east by the Reno basin

<sup>1</sup>Nevada Bureau of Mines and Geology, University of Nevada, Reno, Nevada, USA.

<sup>2</sup>Rosenstiel School of Marine and Atmospheric Science, University of Miami, Miami, Florida, USA.

Corresponding author: J. W. Bell, Nevada Bureau of Mines and Geology, University of Nevada, MS 178, Reno, NV 89557, USA. (jbell@unr.edu)

<sup>1</sup>Auxiliary materials are available in the HTML. doi:10.1029/2012GL052795.

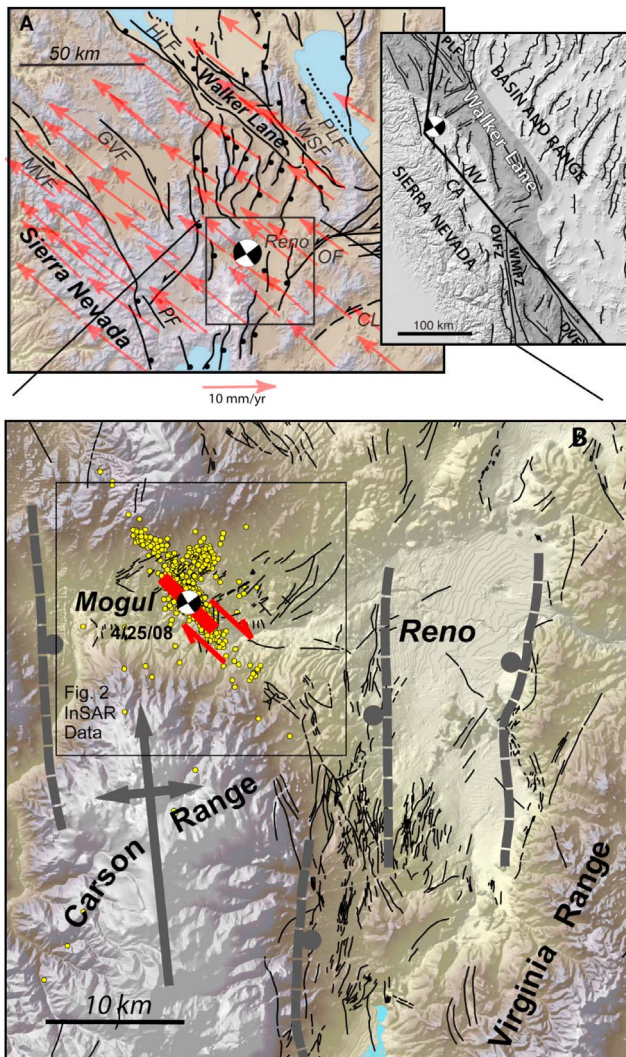


**Figure 1.** Structural setting of the 2008 earthquake swarm. (a) Principal northern Walker Lane faults: Pyramid Lake (PLF), Warm Springs Valley (WSF), Honey Lake (HLF), Mohawk Valley (MVF), Grizzley Valley (GVF), and Polaris (PF) faults. Other Walker Lane faults are sinistral Olinghouse fault (OF) and Carson Lineament (CL). Fault balls indicate extensional faults. GPS velocity field (red arrows) shows that 7–10 mm/a of regional strain is accommodated across the northern Walker Lane [Hammond *et al.*, 2011]. Inset location map shows principal dextral faults of the southern Walker Lane: Death Valley (DVF), White Mountains (WMFZ), and Owens Valley (OVFZ) fault zones. (b) Faults in the Reno basin. Quaternary faults (black (<http://earthquake.usgs.gov/regional/faults>)); InSAR-derived Mogul fault (red); major extensional faults and plunging extensional anticline of the Carson Range (shaded black). Swarm seismicity (yellow) and M 4.7 focal mechanism are from the University of Nevada, Reno Seismological Laboratory. Seismicity is predominantly aligned along a northwest-striking fault trend indicating the preferred nodal plane.

and on the west by east-dipping normal faults [Henry and Perkins, 2001]. The structure of the Reno basin is consistent with solely east-west extension and shows no evidence of Walker Lane style faulting.

[6] East and north of the Reno basin, the northern Walker Lane consists of three principal northwest-striking dextral faults (Honey Lake, Warm Springs Valley, and Pyramid Lake faults; Figure 1a), each having  $\sim 10$  km of post-6 Ma dextral slip based on offset of Tertiary paleovalleys [Faulds *et al.*, 2005] (Figure S2). Farther west, the Mohawk Valley (MVF), Grizzley Valley, and Polaris faults have small dextral displacements totaling less than a few tens of meters [Hunter *et al.*, 2011] (<http://earthquake.usgs.gov/regional/faults>). The MVF had up to 1 km of normal slip; it is a normal fault recently reactivated as a dextral fault. About 7–10 mm/a of contemporary N40W plate motion is accommodated across the region (Figure 1a) [Hammond and Thatcher, 2007; Hammond *et al.*, 2011], possibly on all of these faults. Structure and topography in areas of strike-slip faulting are distinct from those of extension, with northwest-striking ranges, pull-apart basins, and transpressional folds.

### 3. InSAR Data

[7] To search for ground deformation associated with the Mogul swarm, we processed interferograms using C-band radar data acquired by the European Space Agency Envisat satellite. We processed 26 descending pairs and 12 ascending pairs covering both the main event and the foreshock and post-seismic periods (Figure S3). The six best descending and six best ascending unwrapped interferograms (most coherent signals) were then averaged (stacked) to increase the signal-to-noise ratio. Interferograms with poor or partial signal coherence were rejected. Some of the interferograms utilized a common SAR acquisition, and we visually verified using pair-wise logic that the atmospheric delays that may contribute to data uncertainty were absent or minimal.

[8] Although no surface rupture was associated with the swarm, consistent and measureable ground deformation signals were found on interferograms covering the April 25 main event and the aftershock period. Deformation of 0.5–2.5 cm in radar line-of-sight (LOS) was found within a 5–7 km radius of the epicenter, covering a total area of  $\sim 150$  km<sup>2</sup> (Figures 2a and 2b). Comparable, but oppositely facing, LOS decrease lobes occur on the descending and ascending data sets (red lobes in Figures 2a and 2b), owing to the opposing satellite look directions and the strike-slip ground displacement.

### 4. Modeling Results

[9] We used the University of Miami geodetic modeling program *Geodmod* to model fault source parameters from the InSAR data. The program infers tectonic deformation sources from unwrapped InSAR data using an inverse modeling approach. The non-linear inverse problem is solved using a Monte-Carlo-type simulated annealing algorithm [Cervelli *et al.*, 2001] followed by a gradient method [Amelung and Bell, 2003]. Our data points are x and y range displacements sampled on a 400 point grid from the descending and ascending interferogram stacks, assuming unit variance for each data point. For this study, a uniform, single dislocation, elastic half-space model was used [Okada, 1992]. We assumed only that the fault was near-vertical ( $\sim 90^\circ$ ) and strike-slip based on the well-constrained main event focal mechanism [Smith *et al.*, 2008]. Fault slip was otherwise unconstrained, and we estimated the fault length,

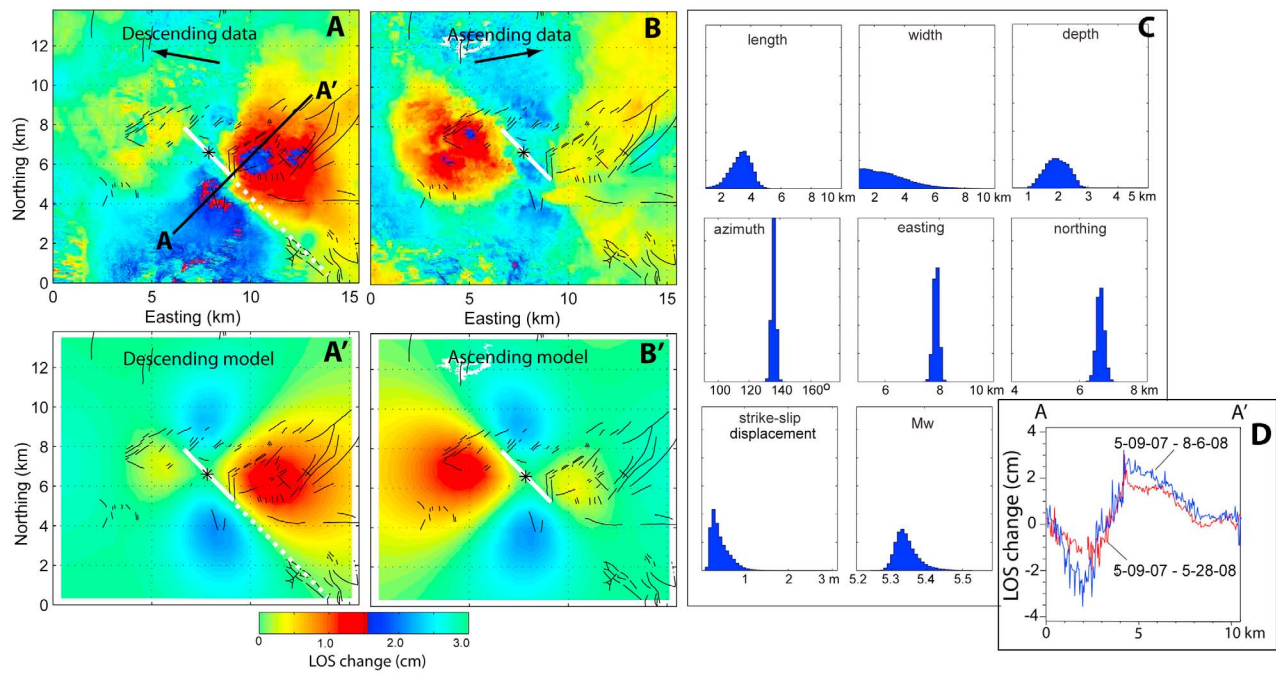


**Figure 2.** Best-fit elastic dislocation fault model for the Mogul earthquake. Quaternary faults shown in black on all figures. Satellite look direction shown by black arrows. (a, a') Descending data stack and model covering period from 5-9-2007 to 7-22-2009. Modeled fault-slip plane shown in white. Main area of LOS decrease [red lobe] lies to the east of the epicenter. (b, b') Ascending data stack and model covering period from 3-26-2007 to 10-26-2009. Main area of LOS decrease (red lobe) lies to the west of the epicenter. (c) Histograms of joint probability density distributions for fault model parameters derived from Gibbs sampling. The moment magnitude is calculated from the fault surface area and displacement using the relation of *Hanks and Kanamori* [1979]. (d) Descending InSAR data transect A–A' showing post-seismic LOS change. Red line shows LOS change for first InSAR pair covering main event (5-9-07 to 5-28-08); blue line shows additional LOS change on the 5-9-07 to 8-6-08 InSAR pair .

width, depth, strike, displacement, epicentral location, and moment magnitude. A Gibbs sampling algorithm was used to estimate joint probability density distributions for these model parameters.

[10] The InSAR data reveal ground deformation from the April 25 main event through the August post-seismic period; no pre-seismic deformation was detected on interferograms covering the February, March, and early April periods. As discussed later, measurable post-seismic deformation occurred, but since the first post-earthquake radar scenes were not acquired until about one month after the main event (May 28 descending scene), it is not possible to precisely determine the co-seismic displacement.

[11] The best-fitting model produces synthetic LOS deformation lobes similar to the deformation data (Figures 2a, 2a', 2b, and 2b'). Gibbs sampling was conducted with up to 100,000 sample sweeps, and a best-fit fault source model was

selected based on comparisons of data-to-model residuals and Gaussian distributions of variable joint probabilities (Figures 2c and S4). The preferred model (Table 1) indicates that the swarm was produced by 25–75 cm of strike-slip displacement on a N44W-striking fault 3.3 km in length, 1–5 km in width, and at a depth of 2.0 km (top of fault plane). The marginal probability density distributions provide insights into whether the model parameters are well constrained by the data (Figure 2c). The fault source parameters have roughly Gaussian distributions except for fault width and strike-slip displacement, which are non-Gaussian, resulting in a strong dependence when varying width or displacement for a given seismic moment. We also obtained identical fault geometry and slip vectors from a model with no fixed variables. Owing to the low signal-to-noise ratio, we used two fixed variables (strike-slip fault; vertical fault plane) in the preferred model to better constrain all other independent variables.

**Table 1.** Model Parameters for Mogul Earthquake (Figure 2c)<sup>a</sup>

Length (km)	Width (km)	Depth (km)	Strike (azimuth)	Dip	Epicenter Easting	Epicenter Northing	Strike-Slip Displacement (m)	Mw
<i>95% Probability Range</i>								
2–4	1–5	1.2–2.5	N42–45 W (135–138)	fixed 90°	7.8–8.0	6.5–6.9	0.25–0.75	5.3–5.4
<i>Preferred Model</i>								
3.3 ± 0.7	NA	2.0 ± 0.4	N44W ± 1 (136 ± 1)	fixed 90°	7.9 ± 0.1	6.6 ± 0.1	NA	5.32

<sup>a</sup>The 95% probability range is inferred from the marginal probability density distributions using Gibbs sampling. The preferred model is the mean of the Gaussian approximations of the probability density distributions; fault width and displacement distributions are not Gaussian and a mean is not defined.

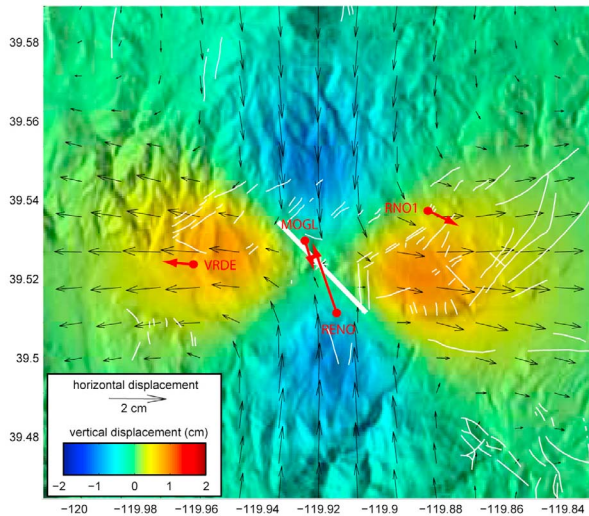


**Figure 3.** InSAR-modeled horizontal and vertical ground deformation. Horizontal displacement vectors (black arrows) show  $\sim 4$  cm of relative across-fault right-lateral movement; vertical displacement ranges from  $-2$  cm to  $+2$  cm. Continuous GPS station vectors (red arrows) are cumulative co- and post-seismic displacements through July, 2008 (University of Nevada Seismological Laboratory, unpublished data, 2008). Stations MOGL and RENO showed 1.1 and 2.9 cm of motion toward each other, more than half of which was post-seismic [Blewitt *et al.*, 2008].

[12] Figure 2c shows the probability density distribution of the modeled moment magnitude ( $M_w$ ) which is calculated from the formulas:

$$\begin{aligned} \text{Seismic moment } M_0 &= \mu DA \\ M_w &= 2/3 \log M_0 - 10.7 \end{aligned}$$

where  $D$  is average displacement,  $A$  is fault area [length  $\times$  width] and  $\mu$  is the rigidity constant  $3 \times 10^{11}$  dyne/cm<sup>2</sup> [Hanks and Kanamori, 1979].

[13] Principal uncertainties in the modeling results are related to low signal-to-noise ratios and coherence on individual interferograms, and to undetected atmospheric phase contributions. The good correlations between most model variables in the joint probability analyses suggest that these effects were minimal.

[14] The modeled ground displacements are in good agreement with continuous GPS observations at four sites (Figure 3) [Blewitt *et al.*, 2008]. The model shows that as much as 4 cm of relative across-fault dextral offset occurred with up to  $\pm 1$  cm of total vertical deformation for the combined main and post-seismic events. Continuous GPS stations RENO and MOGL which straddled the fault also showed similar relative horizontal displacements totaling 4 cm for the swarm. The model-derived horizontal displacement vectors show motions similar to all GPS stations except RNO1, which may have been influenced by a hydrologic signal [Blewitt *et al.*, 2010].

## 5. Seismic and Aseismic Slip Processes

[15] The results demonstrate the capability of InSAR to detect and model small-scale tectonic events that can provide

insights into the larger-scale structural-kinematic processes of the Basin and Range. The InSAR deformation signal is small but measurable, and this is the one of the smallest magnitude earthquakes modeled with InSAR to date in the seismically active western Basin and Range. Inverse modeling indicates that the earthquake and associated after-slip were generated by displacement on a 3-km-long fault rupture.

[16] Our InSAR results indicate that part of the ground deformation was post-seismic, in agreement with continuous GPS data [Blewitt *et al.*, 2008]. GPS stations RENO and MOGL (Figure 3) moved toward each other a total of 4.0 cm by July, 2008 but only 1.5 cm of co-seismic movement occurred on April 25. Successive interferograms covering the April to August periods show greater LOS change indicating post-seismic motion (Figure S5). Although we cannot precisely resolve the same amount of post-seismic displacement, most of the LOS deformation ( $\pm 2$  cm) occurred prior to the May 28 scene followed by  $\pm 1$  cm of additional LOS change by the August 6 scene (Figure 2d). We found similar co-seismic and post-seismic InSAR deformation patterns, indicating that post-seismic slip was occurring as after-slip on the same fault; this is in agreement with conclusions drawn from continuous GPS observations which showed closely aligned co- and post-seismic displacement vectors [Blewitt *et al.*, 2010]. Although several  $M$  3–4 earthquakes preceded the main event, no pre-seismic deformation was detected on the InSAR data, or in the GPS observations [Blewitt *et al.*, 2010].

[17] The model-derived moment magnitude  $M_w$  5.3 for the combined co-seismic and post-seismic signal is larger than the instrumental  $M_w$  5.0 for the main event, and it is also larger than the cumulative moment magnitude for all  $M > 3$  swarm events that we totaled ( $M_w$  5.1). The additional moment required to produce the modeled  $M_w$  5.3 would be roughly equivalent to another  $M_w$  5.0 event suggesting that a significant amount of the post-seismic slip was aseismic. A similar conclusion was drawn from GPS observations [Blewitt *et al.*, 2008]. We do not know whether this aseismic slip is typical of smaller magnitude events in the Basin and Range or whether it is related to the shallow depth of the swarm. Further studies of similar events may provide additional insights into these tectonic processes.

## 6. Westward Migration of Walker Lane Right-Lateral Shear

[18] Our modeling results for the 2008 earthquake swarm support the concept that Walker Lane style dextral faulting is migrating westward into areas of previous extension of the western Basin and Range [Dixon *et al.*, 1995; Lee *et al.*, 2001; Stockli *et al.*, 2003]. The 2008 Mogul swarm occurred on a previously unrecognized N44W-striking dextral fault in a region dominated by north-striking normal faults and long regarded as solely part of the extensional domain of the Sierra Nevada-Basin and Range transition zone [Henry and Perkins, 2001]. No through-going dextral faulting has been previously recognized in the Reno basin. The 2008 fault parallels the principal Walker Lane structures to the east and north, and dextral slip on the N44W fault would result from simple shear within the  $\sim$ N40W northern Walker Lane strain field [Hammond *et al.*, 2011].

[19] Superposition of Walker Lane style faulting on the extensional Reno basin mostly reflects northward propagation and westward encroachment of the youngest part of the Walker Lane system [Faulds *et al.*, 2005; Faulds and Henry, 2008], shown by the 2008 event and the recently reactivated regional normal faults. Initiation of a new N44W Mogul fault may be required because the north-striking normal faults of the Reno basin are too oblique to the modern strain field, whereas the initially normal regional faults (e.g., MVF) are more easily reactivated as dextral faults because they align with the NW-oriented strain field. Similar westward stepping of dextral faulting into regions of prior extension began about 3 Ma in the southern Walker Lane (Figure 1a, inset) [Dixon *et al.*, 1995; Lee *et al.*, 2001; Stockli *et al.*, 2003]; there, dextral slip has been transferred westward from the N40W Death Valley fault system to the new N10–15 W dextral Owens Valley fault and parallel White Mountains fault, an initially 12 Ma normal fault reactivated as right-oblique [Stockli *et al.*, 2003]. Westward migration of right-lateral shear is thus occurring in both southern and northern Walker Lane, with initiation or reactivation influenced by the orientation of older normal faults.

## 7. Conclusions

[20] InSAR analysis and inverse modeling of ground deformation associated with the 2008 M 4.7 ( $M_w$  5.0) Reno-Mogul earthquake swarm indicate that the main event and post-seismic slip were produced by 25–75 cm of dextral slip on a previously unrecognized strike-slip fault in the Reno basin, a region of extension-dominated faulting. Although no surface rupture was produced by the swarm, as much as 2.5 cm of LOS ground deformation was detected within a 150 km<sup>2</sup> area, demonstrating the capability of InSAR to provide insights into the deformation patterns of small-scale tectonic events in the Basin and Range. Our InSAR results support the concept proposed by Stockli *et al.* [2003] that Walker Lane dextral faulting is migrating westward and overprinting the previous extensional structures of the Basin and Range. At Reno, the InSAR results show that the newly recognized strike-slip fault fits this concept, with dextral faulting associated with the northern Walker Lane overprinting extensional fault structures in the Reno basin.

[21] **Acknowledgments.** Envisat radar data were provided from the UNAVCO WInSAR and GeoEarthscope archives; we thank Susanna Gross at UNAVCO for expediting many of our data requests. We appreciate the helpful comments from several anonymous reviewers.

[22] The Editor thanks two anonymous reviewers for assisting in the evaluation of this paper.

## References

- Amelung, F., and J. W. Bell (2003), Interferometric synthetic aperture radar observations of the 1994 Double Spring Flat, Nevada earthquake (M5.9): Main shock accompanied by triggered slip on a conjugate fault, *J. Geophys. Res.*, *108*(B9), 2433, doi:10.1029/2002JB001953.
- Bell, J. W., and L. J. Garside (1987), Geologic map of the Verdi 7 1/2-minute quadrangle, *Map 4Gg*, Nev. Bur. of Mines and Geol., Reno.
- Blewitt, G., J. Bell, W. C. Hammond, C. Kreemer, H. Plag, and C. dePolo (2008), GPS and InSAR monitoring of the Mogul swarm: Evidence for mainly aseismic fault creep with implications for seismic hazard, *Eos Trans. AGU*, *89*(53), Fall Meet. Suppl., Abstract S53C-03.
- Blewitt, G., C. Kreemer, W. W. Hammond, and H.-P. Plag (2010), Separating tectonic, magmatic, hydrological, and landslide signals in GPS measurements near Lake Tahoe, Nevada-California, paper presented at the IGCP 565 Workshop 3: Separating Hydrological and Tectonic Signals in Geodetic Observations, Group on Earth Obs., Reno, Nev., 11–13 Oct.
- Cervelli, P., M. H. Murray, P. Segall, Y. Aoki, and T. Kato (2001), Estimating source parameters from deformation data, with an application to the March 1997 earthquake swarm off the Izu Peninsula, Japan, *J. Geophys. Res.*, *106*, 11,217–11,237, doi:10.1029/2000JB900399.
- dePolo, C. M., D. M. dePolo, and T. M. Garside (2008), Historical earthquake sequences in the western Nevada region—Analogues for the 2008 Mogul-Somerset, Nevada, USA earthquake sequence, *Eos Trans. AGU*, *89*(53), Fall Meet. Suppl., Abstract S51C-1758.
- Dixon, T. H., S. Robaudo, J. Lee, and M. C. Reheis (1995), Constraints on present-day Basin and Range deformation from space geodesy, *Tectonics*, *14*, 755–772, doi:10.1029/95TC00931.
- Faulds, J. E., and C. D. Henry (2008), Tectonic influences on the spatial and temporal evolution of the Walker Lane: An incipient transform fault along the evolving Pacific–North American plate boundary, in *Ores and Orogenesis: Circum-Pacific Tectonics, Geologic Evolution, and Ore Deposits*, edited by J. E. Spencer and S. R. Titley, *Ariz. Geol. Soc. Dig.*, *22*, 437–470.
- Faulds, J. E., C. D. Henry, and N. H. Hinz (2005), Kinematics of the northern Walker Lane: An incipient transform fault along the Pacific–North American plate Boundary, *Geology*, *33*(6), 505–508, doi:10.1130/G21274.1.
- Hammond, W. C., and W. Thatcher (2007), Crustal deformation across the Sierra Nevada, northern Walker Lane, Basin and Range transition, western United States, measured with GPS, 2000–2004, *J. Geophys. Res.*, *112*, B05411, doi:10.1029/2006JB004625.
- Hammond, W. C., G. Blewitt, and C. Kreemer (2011), Block Modeling of crustal deformation of the northern Walker Lane and Basin and Range from GPS velocities, *J. Geophys. Res.*, *116*, B04402, doi:10.1029/2010JB007817.
- Hanks, T. C., and H. Kanamori (1979), A moment-magnitude scale, *J. Geophys. Res.*, *84*, 2348–2350, doi:10.1029/JB084iB05p02348.
- Henry, C. D., and M. E. Perkins (2001), Sierra Nevada–Basin and Range transition near Reno, Nevada: Two stage development at ~12 and 3 Ma, *Geology*, *29*, 719–722, doi:10.1130/0091-7613(2001)029<0719:SNBART>2.0.CO;2.
- Hunter, L. E., J. F. Howle, R. S. Rose, and G. W. Bawden (2011), LiDAR-assisted identification of an active fault near Truckee, California, *Bull. Seismol. Soc. Am.*, *101*, 1162–1181, doi:10.1785/0120090261.
- Lee, J., C. M. Rubin, and A. Calvert (2001), Quaternary faulting history along the Deep Springs fault, California, *Geol. Soc. Am. Bull.*, *113*, 855–869, doi:10.1130/0016-7606(2001)113<0855:QFHATD>2.0.CO;2.
- Massonnet, D., M. Rossi, C. Carmona, F. Adragna, G. Peltzer, K. Feigl, and T. Rabaute (1993), The displacement field of the Landers earthquake mapped by radar interferometry, *Nature*, *364*, 138–142.
- Okada, Y. (1992), Internal deformation due to shear and tensile faults in a half-space, *Bull. Seismol. Soc. Am.*, *82*, 1018–1040.
- Smith, K., D. H. von Seggern, D. dePolo, J. G. Anderson, G. P. Biasi, and R. Anoshpooor (2008), Seismicity of the 2008 Mogul-Somerset, West Reno, Nevada earthquake sequence, *Eos Trans. AGU*, *89*(53), Fall Meet. Suppl., Abstract S53C-02.
- Stewart, J. H. (1988), Tectonics of the Walker Lane belt, western Great Basin: Mesozoic and Cenozoic deformation in a zone of shear, in *Metamorphism and Crustal Evolution of the Western United States*, Rubey, vol. 7, edited by W. G. Ernst, pp. 683–713, Prentice Hall, Englewood Cliffs, N. J.
- Stockli, D. F., T. A. Dumitru, M. O. McWilliams, and K. A. Farley (2003), Cenozoic tectonic evolution of the White Mountains, California and Nevada, *Geol. Soc. Am. Bull.*, *115*, 788–816, doi:10.1130/0016-7606(2003)115<0788:CTEOTW>2.0.CO;2.